







# THE INFRARED LUMINOSITY OF RETIRED AND POST-STARBURST GALAXIES: A CAUTIONARY TALE FOR STAR FORMATION RATE MEASUREMENTS

VIVIENNE WILD <sup>1\*</sup>, NATALIA VALE ASARI <sup>2</sup>, KATE ROWLANDS <sup>3</sup>, SARA L. ELLISON <sup>4</sup>,  
HO-HIN LEUNG <sup>1</sup>, CHRISTY TREMONTI <sup>5</sup>

<sup>1</sup>School of Physics & Astronomy, University of St Andrews, North Haugh, St Andrews, KY16 9SS, U.K.

<sup>2</sup>Departamento de Física-CFM, Universidade Federal de Santa Catarina, C.P. 5064, 88035-972, Florianópolis, SC, Brazil

<sup>3</sup>AURA for ESA, Space Telescope Science Institute, 3700 San Martin Drive, Baltimore, MD 21218, USA; William H. Miller III

Department of Physics and Astronomy, Johns Hopkins University, Baltimore, MD 21218, USA

<sup>4</sup>Department of Physics & Astronomy, University of Victoria, Finnerty Road, Victoria, British Columbia, V8P 1A1, Canada

<sup>5</sup>Department of Astronomy, University of Wisconsin-Madison, Madison, WI 53706, USA

Version January 9, 2025

## ABSTRACT

In galaxies with significant ongoing star formation there is an impressively tight correlation between total infrared luminosity ( $L_{\text{TIR}}$ ) and  $\text{H}\alpha$  luminosity ( $L_{\text{H}\alpha}$ ), when  $\text{H}\alpha$  is properly corrected for stellar absorption and dust attenuation. This long-standing result gives confidence that both measurements provide accurate estimates of a galaxy’s star formation rate (SFR), despite their differing origins. To test the extent to which this holds in galaxies with lower specific SFR ( $\text{sSFR} = \text{SFR}/M_*$ , where  $M_*$  is the stellar mass), we combine optical spectroscopy from the Sloan Digital Sky Survey (SDSS) with multi-wavelength (FUV to FIR) photometric observations from the Galaxy And Mass Assembly survey (GAMA). We find that  $L_{\text{TIR}}/L_{\text{H}\alpha}$  increases steadily with decreasing  $\text{H}\alpha$  equivalent width ( $W_{\text{H}\alpha}$ , a proxy for sSFR), indicating that both luminosities cannot provide a valid measurement of SFR in galaxies below the canonical star-forming sequence. For both ‘retired galaxies’ and ‘post-starburst galaxies’,  $L_{\text{TIR}}/L_{\text{H}\alpha}$  can be up to a factor of 30 larger than for star-forming galaxies. The smooth change in  $L_{\text{TIR}}/L_{\text{H}\alpha}$ , irrespective of star formation history, ionisation or heating source, dust temperature or other properties, suggests that the value of  $L_{\text{TIR}}/L_{\text{H}\alpha}$  is determined by the balance between star-forming regions and ambient interstellar medium contributing to both  $L_{\text{TIR}}$  and  $L_{\text{H}\alpha}$ . It is not a result of the differing timescales of star formation that these luminosities probe. While  $L_{\text{H}\alpha}$  can only be used to estimate the SFR for galaxies with  $W_{\text{H}\alpha} > 3 \text{ \AA}$  ( $\text{sSFR} \gtrsim 10^{-11.5}/\text{yr}$ ), we argue that the mid- and far-infrared can only be used to estimate the SFR of galaxies on the star-forming sequence, and in particular only for galaxies with  $W_{\text{H}\alpha} > 10 \text{ \AA}$  ( $\text{sSFR} \gtrsim 10^{-10.5}/\text{yr}$ ). We find no evidence for dust obscured star-formation in local post-starburst galaxies.

**Keywords:** galaxies: evolution – galaxies: star formation – galaxies: starburst – galaxies: stellar content.

## 1. INTRODUCTION

Measuring the rate at which galaxies form stars is one of the key tools used to understand how they form and evolve. The field has benefited from a wide range of independent methods, from data spanning the full electro-magnetic spectrum, allowing for internal consistency checks and validation (see Kennicutt & Evans 2012, for a review). This has led to significant confidence amongst extra-galactic astronomers in our ability to accurately measure the star formation rate (SFR) of any galaxy, of any type, at any redshift, with important caveats often under-appreciated.

Here we focus on one particular relation, between total infrared (TIR) luminosity (including mid- and far-IR) and  $\text{H}\alpha$  luminosity. Once  $\text{H}\alpha$  has been properly corrected for stellar photospheric Balmer absorption and for dust attenuation via the Balmer decrement method,

the two luminosities are impressively tightly correlated in local star-forming galaxies (Rosa-González et al. 2002; Kewley et al. 2002; Rosario et al. 2016), despite their different physical origins. Balmer emission lines are produced via recombination of electrons to the  $n = 2$  level of the hydrogen atom; in star-forming galaxies this predominantly occurs following photoionisation and subsequent recombination and cascade within the  $\text{H II}$  regions that surround hot (O and B type) stars. Mid to far-IR emission is caused by the heating of dust grains through the absorption of ultra-violet (UV) to optical photons. In highly star-forming galaxies these photons come predominantly from young, hot stars and interact with the dense, dust rich birth clouds of the star forming regions, leading to the strong relation between TIR emission and SFR. Unfortunately, neither of these SFR estimators are free of contamination or complications.

The basic physics of Balmer emission in star-forming galaxies is simple and well understood, with only pho-

\*vw8@st-andrews.ac.uk

tons with energies greater than 13.6 eV (Lyman continuum photons) able to contribute to the ionisation of the hydrogen atoms in the first place, meaning O and B stars are the primary contributor to Balmer emission in star-forming galaxies. However, there are two key complications in converting a  $H\alpha$  emission line luminosity into a SFR. These are the attenuation of the photons as they travel through the galaxy ISM once leaving the  $H\text{ II}$  regions, and the contribution to the far-UV interstellar radiation field (ISRF) from active galactic nuclei (AGN), shocks and hot low-mass evolved stars (HOLMES; Flores-Fajardo et al. 2011), such as hot post-asymptotic giant branch stars and white dwarfs (Stasińska et al. 2008; Cid Fernandes et al. 2011). Through modelling the stellar continuum in SDSS galaxies using population synthesis models, Cid Fernandes et al. (2011) showed that galaxies with a low equivalent width of the  $H\alpha$  emission line ( $W_{H\alpha} < 3\text{ \AA}$ ) had an ionisation source consistent with the HOLMES present in the galaxy continuum spectrum, calling them ‘retired galaxies’. In these galaxies  $L_{H\alpha}$  is not proportional to their SFR, but is proportional to the total stellar mass of lower mass stars available to provide the ionising photons, as well as the presence of a reservoir of warm gas (see Herpich et al. 2018, for a comparison of retired galaxies with and without  $H\alpha$  emission).

Once the  $H\alpha$  photon is emitted from the  $H\text{ II}$  region close to the site of star formation, it can be absorbed and scattered by dust within the galaxy before being received by our telescopes<sup>1</sup>. In the case that *some* of the line emission still escapes and the dust distribution in the galaxy is smooth, the loss of light can be corrected for via the known ratio between Balmer line fluxes, combined with a knowledge of the dust attenuation as a function of wavelength (the Balmer decrement method, see e.g. Groves et al. 2012). In the case of clumpy dust the detected Balmer emission is weighted towards lower dust regions, and therefore the dust attenuation in the galaxy is underestimated using this method (Vale Asari et al. 2020). Comparison between spatially resolved and integrated light observations indicate that this effect is at the  $\lesssim 10\%$  level in the majority of galaxies (Vale Asari et al. 2020; Belfiore et al. 2023), however the relative lack of very high spatial resolution integral field spectroscopy makes this estimate uncertain. At the extreme end of this scenario, there is clearly no way to correct for Balmer emission that has been entirely blocked by dense dust clouds.

On the other hand, the physics of mid- to far-IR luminosity is highly complex, with dependence on the gas density, dust-star geometry, the distribution of dust grain sizes and types which can vary with metallicity, and the shape of the ISRF, which depends on the stellar popula-

tion balance (e.g. Draine & Li 2007; Paladini et al. 2007; Bernard et al. 2010; Nersesian et al. 2019). It is predominantly the strong correlation with other measurements that provides the evidence for the link between TIR and SFR in high SFR galaxies. While Balmer emission lines are somewhat impacted by HOLMES, significant dust heating is caused by all stars with masses below O and B type stars. Diffuse dust emission permeates the entire galaxy contributing significantly to the IR luminosity of galaxies or regions with lower ongoing SFRs (e.g. Helou 1986; Lonsdale Persson & Helou 1987; Paladini et al. 2007; Bendo et al. 2010; Kennicutt et al. 2011; Calzetti 2013; Nersesian et al. 2019). As a result, the TIR to  $H\alpha$  luminosity ratio ( $L_{\text{TIR}}/L_{H\alpha}$ ) has been observed to increase with decreasing specific SFR ( $\text{sSFR} = \text{SFR}/M_*$ , where  $M_*$  is a galaxy’s stellar mass) in integrated SDSS–Herschel (Rosario et al. 2016) and SDSS–WISE (Salim et al. 2016) comparisons, and spatially resolved PHANGS–MUSE comparisons (Belfiore et al. 2023). While Rosario et al. (2016) put the effect down to selection bias, Belfiore et al. (2023) interpreted it as due to contamination of the IR luminosity by diffuse ISM dust.

The fact that there may be significant reservoirs of dust invisible to optical astronomers due to the enormous optical depths of stellar birth clouds has led to the idea that FIR may in fact be a *better* indicator of SFR in certain types of galaxies. This has become a critical discussion in particular in relation to galaxies which are currently shutting down their star formation (so-called ‘quenching’), and has crucial importance as the field grapples with understanding the wide range of processes that cause galaxies to stop forming stars. If the dust in a galaxy is sufficiently dense to bury light from a significant number of the O and B stars, as well as their surrounding  $H\text{ II}$  regions, then we have the case of a ‘dust obscured starburst’. Such a galaxy may reveal its presence in the optical via strong Balmer absorption lines, as the longer living A and F stars emerge from the dense clouds shrouding the younger O and B stars (Smail et al. 1999; Poggianti & Wu 2000; Geach et al. 2009; Baron et al. 2022).

However, an excess Balmer absorption line strength is exactly the signature used to detect galaxies which have recently and rapidly shut down their star formation. Ironically, it is in these rapidly quenching galaxies where we might also expect to see the largest fraction of IR dust emission coming from the ambient ISM, unrelated to current star formation, as clearly demonstrated using hydrodynamical merger simulations by Hayward et al. (2014). This is because (a) we expect the diffuse dust emission located far from previous sites of star formation to still be present, (b) there is significant UV–optical light emitted by the A and F stars, (c) these A and F stars may also still be co-located with the remnant dust from the starburst episode. So while  $H\alpha$  disappears rapidly following the starburst, total IR luminosity is expected to remain high, leading to an order of magnitude

<sup>1</sup> We are ignoring here the possibility that dust grains within the  $H\text{ II}$  region might absorb the photon before it ever reaches the hydrogen atoms to ionise them. Such competition for Lyman continuum photons is difficult to detect (e.g. Charlot & Longhetti 2001; Murphy et al. 2011).

over-estimation in star formation, if using IR luminosity, from the point at which star formation starts to decline, right into the quenched phase many 100's of Myr later (see figures 2 and 3 of [Hayward et al. 2014](#)).

As the debate about the role of total IR emission as a SFR indicator in quenching galaxies continues, and the origin of IR emission in ‘retired’ galaxies has not yet been studied, this paper takes a fresh look at the relationship between total IR luminosity and  $H\alpha$  luminosity in a wide range of galaxies, including star-forming, post-starburst and retired galaxies. In Section 2 we present the catalogues that we have combined in our analysis, in Section 3 we summarise the relevant methods, and in Section 4 we present our results. We discuss our results with the help of a simple toy model in Section 5 and summarise in Section 6. Throughout the paper we assume a cosmology of  $\Omega_M = 0.3$ ,  $\Omega_\Lambda = 0.7$  and  $h = 0.7$  when converting fluxes into luminosity. All derived catalogues that we use assume a [Chabrier \(2003\)](#) initial mass function for conversion of stellar light into stellar masses. Unless otherwise stated  $L_{H\alpha}$  refers to dust attenuation and aperture corrected  $H\alpha$  luminosity.

## 2. DATA

Our analysis requires a large sample of galaxies with good quality optical continuum spectroscopy to provide continuum subtracted, dust attenuation corrected  $H\alpha$  luminosity, combined with aperture-matched UV, optical and mid- to far-IR multiwavelength photometric observations to provide accurate dust luminosities. To this end, we combine the spectroscopic galaxy sample from the Sloan Digital Sky Survey (SDSS) Data Release 7 (DR7, [Abazajian et al. 2009](#)), with photometry from the Galaxy And Mass Assembly (GAMA) Data Release 4 equatorial survey ([Driver et al. 2022](#)).

From SDSS we take nebular emission line fluxes, errors and equivalent widths from the STARLIGHT–SDSS catalogue ([Cid Fernandes et al. 2009](#); see also [Mateus et al. 2006](#); [Stasińska et al. 2006](#); [Asari et al. 2007](#); [Cid Fernandes et al. 2010](#)). The underlying stellar continuum is subtracted prior to measurement of the emission line fluxes using the STARLIGHT full spectral fitting package ([Cid Fernandes et al. 2005](#)). Stellar masses are calculated from the mass-to-light ratio of the STARLIGHT model, and corrected for aperture loss using the fiber-to-total  $z$ -band luminosity fraction. The luminosity of the  $H\alpha$  emission line is corrected for dust attenuation using the [Cardelli et al. \(1989\)](#) law with  $R_V = 3.1$  and assuming an intrinsic Balmer decrement of  $H\alpha/H\beta = 2.86$ . This steeper dust law than e.g. [Calzetti et al. \(2000\)](#) is appropriate for correcting emission lines, due to the screen-like geometry of the dust in  $H\text{ II}$  regions ([Wild et al. 2007](#); [da Cunha et al. 2008](#); [Wild et al. 2011](#)). While the assumed dust law alters the absolute conversion between  $L_{H\alpha}$  and  $L_{\text{TIR}}$  in the case that both trace SFR, this does not impact the conclusions of this paper.

From GAMA we obtain 21 band multi-wavelength photometry from the LAMBDA catalogues ([Wright et al.](#)

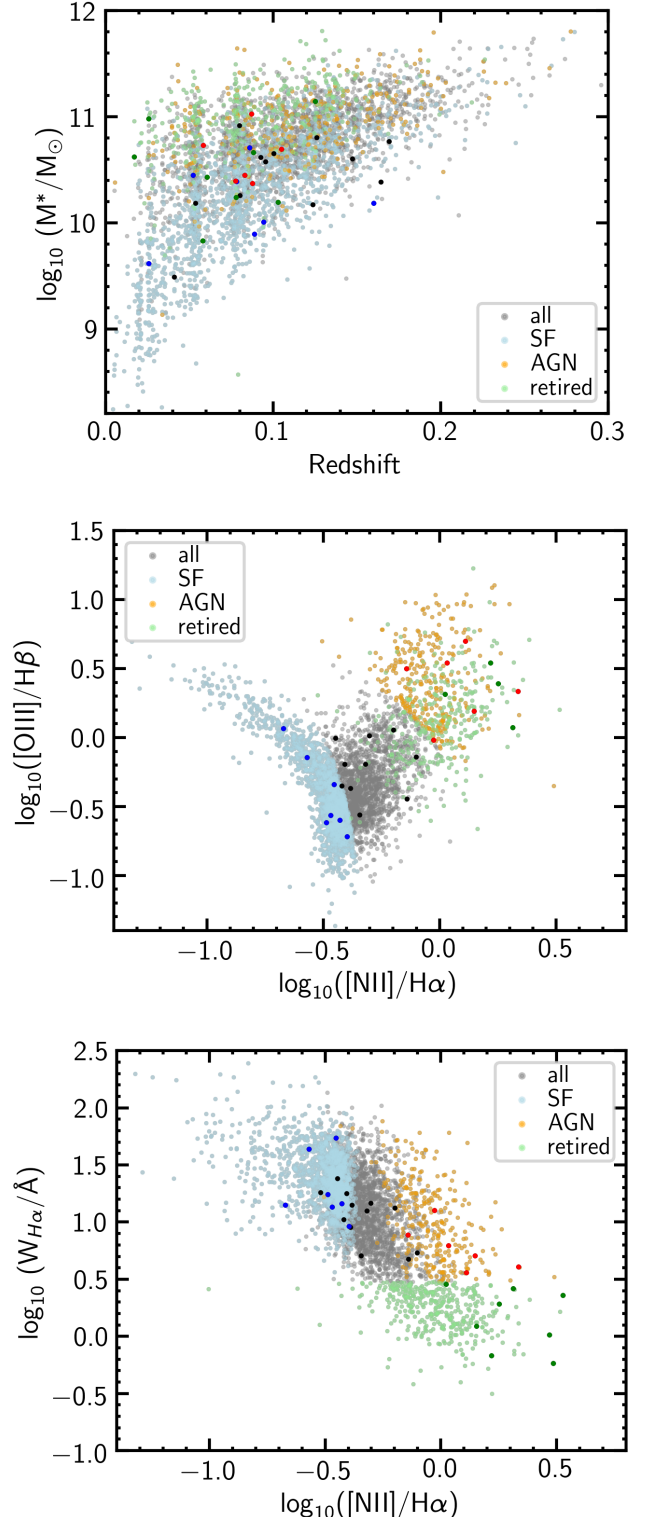


**Figure 1.** A summary of the properties of the galaxies studied in this paper. Galaxies are colour coded according to their emission line properties into star-forming (SF), AGN and retired galaxies, as described in the text. Post-starburst galaxies are identified via their stellar continuum properties, and are shown as darker coloured circles. *Top:* redshift vs. total stellar mass. *Centre:*  $[N\text{ II}]/H\alpha$  vs.  $[O\text{ III}]/H\beta$  line flux ratios. *Bottom:*  $[N\text{ II}]/H\alpha$  line flux ratio vs. the equivalent width of the  $H\alpha$  emission line.

2016), which is aperture-matched and deblended, with variations in the point-spread function and pixel scale across the various bands properly accounted for (see also Driver et al. 2016). Most importantly for this paper, the GAMA equatorial fields include observations from Data Release 1 of the Herschel–ATLAS far-IR space telescope survey (H-ATLAS, Valiante et al. 2016; Bourne et al. 2016), and the Wide Field Infrared Survey Explorer which covers the mid-IR (WISE, Wright et al. 2010; Cluver et al. 2014). These two surveys provide 6 band photometry across the crucial 22–500  $\mu\text{m}$  wavelength range<sup>2</sup> required to measure and characterise the emission from dust in galaxies. The majority of the galaxies in our sample also have GALEX NUV and FUV fluxes detected at  $> 3\sigma$ , including the post-starburst and retired galaxies. The latter are typically detected with lower significance. We make use of the GAMA DR4 MAGPHYS catalogue, which takes input photometry from the LAMBDAR catalogue using the code of da Cunha et al. (2008) to measure stellar population and dust properties for GAMA galaxies.

### 2.1. Sample selection

From the SDSS spectroscopic main galaxy sample (PRIMTARGET = 64, Strauss et al. 2002) we exclude a small number of objects for which the SDSS 1D spectroscopic pipeline has identified problems, i.e. if the Z\_WARNING flag is set, or the velocity dispersion is fitted to the maximum value of  $V_{\text{DISP}} = 850 \text{ km s}^{-1}$  (Stoughton et al. 2002). We use TOPCAT (Taylor 2005) to match the SDSS and GAMA galaxies, using the catalogue right ascension and declination values and requiring an on-sky separation of  $< 0.5''$ . This results in a parent sample of 12,738 galaxies.

The GAMA MAGPHYS catalogue contains dust emission parameters even for galaxies with no mid- or far-IR photometric detections; these are predictions based on the MAGPHYS model priors. We therefore restrict our analysis to only those galaxies with  $\geq 2$  photometric bands between 22–500  $\mu\text{m}$  detected at  $> 3\sigma$  in the LAMBDAR catalogue. This reduces the sample to 4,368 galaxies. Finally, we restrict our sample to objects with  $\text{H}\alpha$  detected at  $> 5\sigma$ , leading to a final sample of 4,121 galaxies with SDSS spectroscopy, GAMA photometry, H-ATLAS/WISE and  $\text{H}\alpha$  emission line detections.

#### 2.1.1. Star-forming and retired samples

Of these 4,121 galaxies, we find that 1,638 galaxies have optical emission line ratios that indicate the gas is solely ionised by young stellar populations, using the criteria of Stasińska et al. (2006), which is based on the commonly used  $[\text{N II}]/\text{H}\alpha$  and  $[\text{O III}]/\text{H}\beta$  line flux ratios. We find that 386 galaxies have  $\text{H}\alpha$  equivalent widths  $W_{\text{H}\alpha} < 3\text{\AA}$ , the limit below which a galaxy is classified as ‘retired’ i.e. the emission lines are consistent with

the ionisation source being hot low-mass evolved stars (HOLMES) present in the galaxy continuum spectrum (Cid Fernandes et al. 2011). We also find 305 galaxies are classified as AGN using the Kewley et al. (2001) criteria. The ionising photons responsible for the  $\text{H}\alpha$  emission in the remaining galaxies likely come from a mixture of HOLMES, ongoing star formation, shocks and low luminosity AGN. For the purposes of this paper it is essential to include galaxies with all ionisation sources, but we refrain from converting  $L_{\text{H}\alpha}$  into SFR for our figures. Figure 1 shows the samples in stellar mass vs. redshift, and on standard emission line diagnostic diagrams.

#### 2.1.2. Post-starburst sample

There are many ways to identify post-starburst galaxies, although all methods are based around identifying galaxies with an excess of A/F stars compared to their O/B star population, indicating a recent and rapid shut-off in star formation. Traditionally a complete absence of nebular emission lines was used to provide evidence for a lack of O/B stars (e.g. Dressler & Gunn 1983; Couch & Sharples 1987; Zabludoff et al. 1996; Goto et al. 2003). However, this method excludes the many interesting post-starburst galaxies with residual ongoing star formation and other ionisation sources. Therefore, most modern methods use an alternative method to determine a deficit of O/B stars relative to the A/F star population, such as information from the stellar continuum shape, the equivalent width of one of the emission lines, likely ionisation sources of the emission lines or longer wavelength photometry (Wild et al. 2007; Yan et al. 2009; Alatalo et al. 2016; Yesuf et al. 2017).

Due to our requirement for significant  $\text{H}\alpha$  emission line flux, as well as mid- and far-IR photometric detections, we note that the post-starburst sample studied in this paper is biased to include only post-starburst galaxies with a significant interstellar medium, as well as sources to heat and ionise it, such as residual star-formation, shocks, HOLMES or AGN. However, as it is predominantly these galaxies which are argued to be dusty starburst interlopers in quenching samples (e.g. Poggianti & Wu 2000; Baron et al. 2022), they are the relevant objects for this analysis.

We match our combined SDSS+GAMA+H-ATLAS/WISE sample onto several SDSS DR7 post-starburst samples in the literature, identifying 33 post-starburst galaxies in total. Positions, catalogue identifiers and basic properties for these galaxies are given in Table 1. The sample includes 3 galaxies from Goto (2007), 24 from Wild et al. (2007)<sup>3</sup>, 4 from Alatalo et al. (2016), 7 from Pattarakijwanich et al. (2016) and 9 applying the method described in Chen et al. (2019) to SDSS DR7, referred to as the ‘Tremonti sample’. Some

<sup>2</sup> i.e. WISE W4, PACS 100, PACS 160, SPIRE 250, SPIRE 350, SPIRE 500.

<sup>3</sup> We follow Pawlik et al. (2018) and exclude dusty PCA-selected post-starburst candidates with  $\text{H}\alpha/\text{H}\beta$  ratios  $> 6.6$ . These are possible contaminants for this particular method, due to the impact of significant dust attenuation on the shape of the stellar continuum.



**Table 1**  
Position, catalogue identifiers and basic properties of the post-starburst galaxies studied in this paper.

| RA<br>°   | Dec<br>° | Plate | MJD   | Fiberid | GAMA-DR4<br>CATAID | Catalogues | $z$   | $M_*$<br>dex( $M_\odot$ ) | $L_{H\alpha}$<br>dex( $L_\odot$ ) | $L_{TIR}$<br>dex( $L_\odot$ ) | $W_{H\alpha}$<br>Å |
|-----------|----------|-------|-------|---------|--------------------|------------|-------|---------------------------|-----------------------------------|-------------------------------|--------------------|
| 130.77146 | 1.14878  | 467   | 51901 | 397     | 300757             | 5          | 0.078 | 10.4                      | 7.6                               | 10.8                          | 4.1                |
| 133.40527 | 1.71763  | 469   | 51913 | 338     | 323854             | 2          | 0.058 | 10.7                      | 8.3                               | 10.4                          | 7.7                |
| 134.17632 | 1.03737  | 468   | 51912 | 557     | 372076             | 2          | 0.088 | 10.7                      | 7.4                               | 9.9                           | 2.9                |
| 135.19133 | -0.49369 | 470   | 51929 | 290     | 550327             | 2          | 0.041 | 9.5                       | 7.6                               | 10.1                          | 24.0               |
| 135.50417 | -0.56457 | 470   | 51929 | 251     | 550389             | 2          | 0.089 | 9.9                       | 7.6                               | 10.4                          | 14.6               |
| 135.88658 | 1.21010  | 470   | 51929 | 402     | 372446             | 2,4,5      | 0.058 | 9.8                       | 6.1                               | 9.5                           | 0.6                |
| 136.75280 | 0.06094  | 470   | 51929 | 115     | 210106             | 2,5        | 0.164 | 10.4                      | 7.8                               | 10.6                          | 4.8                |
| 137.33520 | 0.73873  | 470   | 51929 | 621     | 623161             | 2          | 0.054 | 10.2                      | 7.6                               | 9.8                           | 12.5               |
| 139.67269 | 2.02517  | 473   | 51929 | 464     | 383051             | 2          | 0.087 | 11.0                      | 8.2                               | 10.7                          | 6.3                |
| 140.82538 | 0.56146  | 474   | 52000 | 408     | 217011             | 2          | 0.088 | 10.4                      | 7.9                               | 9.9                           | 3.6                |
| 140.90214 | 2.13637  | 473   | 51929 | 593     | 383312             | 2          | 0.017 | 10.6                      | 7.5                               | 10.3                          | 1.9                |
| 140.92896 | 1.34917  | 473   | 51929 | 29      | 373374             | 2          | 0.025 | 11.0                      | 6.7                               | 10.0                          | 1.2                |
| 177.64780 | -2.63937 | 329   | 52056 | 117     | 123917             | 3          | 0.093 | 10.6                      | 7.9                               | 10.5                          | 13.3               |
| 177.65639 | 1.50016  | 515   | 52051 | 295     | 397294             | 1,2,4,5    | 0.078 | 10.2                      | 6.5                               | 9.9                           | 1.0                |
| 178.10642 | -1.26744 | 330   | 52370 | 361     | 143889             | 1,2,5      | 0.060 | 10.4                      | 6.5                               | 10.1                          | 2.3                |
| 179.98362 | -0.68304 | 285   | 51663 | 162     | 40161              | 4          | 0.080 | 10.3                      | 7.6                               | 10.1                          | 10.6               |
| 180.74100 | 0.05999  | 286   | 51999 | 395     | 70638              | 2,4        | 0.080 | 10.9                      | 8.0                               | 10.5                          | 9.0                |
| 181.11809 | -0.88879 | 286   | 51999 | 208     | 536202             | 2          | 0.094 | 10.0                      | 8.4                               | 10.4                          | 43.5               |
| 181.22794 | 0.31118  | 286   | 51999 | 477     | 610664             | 1          | 0.100 | 10.7                      | 7.8                               | 10.6                          | 5.1                |
| 181.43242 | 1.07895  | 286   | 51999 | 444     | 23386              | 4          | 0.086 | 10.7                      | 7.8                               | 10.5                          | 9.2                |
| 181.62258 | -0.55774 | 286   | 51999 | 150     | 560745             | 2          | 0.095 | 10.6                      | 8.1                               | 10.6                          | 5.4                |
| 182.43333 | -0.28872 | 286   | 51999 | 78      | 55486              | 2          | 0.160 | 10.2                      | 8.6                               | 11.0                          | 54.5               |
| 182.70929 | 0.47087  | 286   | 51999 | 634     | 85480              | 4          | 0.078 | 10.4                      | 7.9                               | 10.3                          | 13.5               |
| 183.03908 | -1.68483 | 332   | 52367 | 527     | 138549             | 2,5        | 0.103 | 10.2                      | 6.4                               | 9.8                           | 0.7                |
| 212.55941 | -0.57859 | 302   | 51688 | 110     | 567624             | 3          | 0.026 | 9.6                       | 6.9                               | 9.2                           | 14.2               |
| 213.29913 | -0.39941 | 304   | 51609 | 291     | 62531              | 3          | 0.126 | 10.8                      | 8.1                               | 10.7                          | 14.6               |
| 214.16447 | 1.30599  | 533   | 51994 | 55      | 227568             | 2          | 0.123 | 10.2                      | 8.2                               | 10.3                          | 17.8               |
| 214.19902 | -1.07059 | 303   | 51615 | 89      | 37000              | 2,3,5      | 0.125 | 11.1                      | 8.7                               | 10.6                          | 2.6                |
| 214.46337 | -0.13896 | 304   | 51609 | 216     | 592879             | 4          | 0.169 | 10.8                      | 8.3                               | 10.6                          | 14.1               |
| 216.59955 | 2.26955  | 535   | 51999 | 341     | 342615             | 2,5        | 0.105 | 10.7                      | 8.2                               | 10.6                          | 12.6               |
| 216.81288 | 0.93103  | 306   | 51637 | 321     | 106634             | 2          | 0.052 | 10.4                      | 7.8                               | 10.1                          | 17.4               |
| 221.69920 | -1.21974 | 920   | 52411 | 460     | 493601             | 2,5        | 0.083 | 10.4                      | 8.3                               | 10.4                          | 5.1                |
| 223.07965 | 0.13545  | 308   | 51662 | 638     | 79784              | 2          | 0.147 | 10.6                      | 7.9                               | 10.8                          | 18.1               |

Catalogue references: (1) Goto (2007) (2) Wild et al. (2007); (3) Alatalo et al. (2016); (4) Pattarakijwanich et al. (2016); (5) C. Tremonti and Chen et al. (2019).

objects are identified using multiple methods, with the largest cross over being 8 objects contained in both the Wild et al. (2007) and Tremonti samples. The selection criteria of each sample is summarised in Table 2.

The sample includes 7 post-starburst galaxies where optical emission lines indicate that the dominant ionising source is residual star-formation (below the demarcation line of Stasińska et al. 2006), 8 are consistent with being ionised by HOLMES ( $W_{H\alpha} < 3 \text{ Å}$ ), 6 ionised by AGN (above the demarcation line of Kewley et al. 2001 and  $W_{H\alpha} > 3 \text{ Å}$ ), and 10 lie between the Stasińska et al. (2006) and Kewley et al. (2001) demarcation lines of the [N II]/H $\alpha$  and [O III]/H $\beta$  line ratios diagram (Baldwin et al. 1981). The post-starburst galaxies are shown with darker coloured symbols in Figure 1.

### 3. METHODS

Here we summarise the relevant data analysis and interpretation methods used in this paper.

*Partial correlation coefficients:* Throughout the results section we use partial correlation coefficients to quantify the correlation between three variables. For variables ( $x$ ,  $y$  and  $z$ ) we firstly compute the Spearman rank-order correlation coefficient between each:  $\rho_{xy}$ ,  $\rho_{xz}$  and  $\rho_{yz}$ . The partial correlation between  $x$  and  $z$ , given  $y$ , is then:

$$\rho_{xz|y} = \frac{\rho_{xz} - \rho_{xy}\rho_{zy}}{\sqrt{(1 - \rho_{xy}^2)}\sqrt{(1 - \rho_{zy}^2)}}. \quad (1)$$

The angle of the correlation with  $z$ , projected onto the  $x$ - $y$  plane ( $\theta_p$ ), is given by:

$$\tan \theta_p = \frac{\rho_{xz|y}}{\rho_{yz|x}}. \quad (2)$$

**Table 2**

Comparison between the different selection methods of post-starburst galaxies included in this paper. In order to distinguish absorption from emission in this table, equivalent width values ( $W$ ) follow the convention of positive for absorption and negative for emission. Note that in the remainder of the paper we use absolute equivalent width values for  $W_{H\alpha}$  in emission.

| Author  | Survey                | Balmer absorption lower limit  | Ongoing SFR upper limit   |
|---|-----------------------|--|---|
| <a href="#">Goto (2007)</a>                         | SDSS DR5              | $W_{H\delta} > 5 \text{ \AA}$  | $W_{H\alpha} > -3 \text{ \AA}$ and $W_{[O\text{II}]} > -2.5 \text{ \AA}^a$                    |
| <a href="#">Wild et al. (2007)</a>                  | SDSS DR7              | PC2 > 0.025 and PC1 < -1.5<br>(i.e. excess Balmer absorption compared to 4000 Å break strength) <sup>b</sup> |   |
| <a href="#">Alatalo et al. (2016)</a>               | SDSS DR7              | $W_{H\delta} > 5 \text{ \AA}$  | Line ratios consistent with shock ionisation and inconsistent with star-formation ionisation. |
| <a href="#">Pattarakijwanich et al. (2016)</a>      | SDSS DR9 <sup>c</sup> | Template fitting <sup>d</sup> $A/(A+K) > 0.25$ and $W_{H\delta} > 4 \text{ \AA}$                             | $W_{[O\text{II}]} > -2.5 \text{ \AA}$   |
| Tremonti sample; <a href="#">Chen et al. (2019)</a> | SDSS DR7              | $H\delta_A > 3 \text{ \AA}^e$  | $W_{H\alpha} > -10 \text{ \AA}$ and $\log_{10}  W_{H\alpha}  < 0.23 \times H\delta_A - 0.46$  |

<sup>a</sup>Lines measured with flux summing method ([Goto et al. 2003](#)).

<sup>b</sup>Additional cut on Balmer decrement ([Pawlik et al. 2018](#)).

<sup>c</sup>Sample restricted to DR7 only in this paper.

<sup>d</sup>Method from [Quintero et al. \(2004\)](#).

<sup>e</sup>Lick Index ([Worthey & Ottaviani 1997](#)).

An angle of  $45^\circ$  indicates the  $z$  quantity correlates equally with the  $x$  and  $y$  quantities;  $0^\circ$  indicates the  $z$  quantity correlates with  $y$  alone;  $90^\circ$  indicates the  $z$  quantity correlates with  $x$  alone;  $-45^\circ$  indicates the  $z$  quantity correlates equally with the  $x$  and with  $y$ , but an increase in  $x$  corresponds to a decrease in  $y$ .

*Expected luminosity ratio:* We compare our observed ratio between the luminosities of  $H\alpha$  and total IR (TIR), to the ratio expected if both quantities measure SFR. Following the notation of [Kennicutt & Evans \(2012\)](#),  $\log_{10}(\text{SFR}) = \log_{10}(L_X) - \log_{10}(C_X)$ , with SFR in  $M_\odot/\text{yr}$  and luminosities in  $\text{erg/s}$ . With  $C = 43.41$  for TIR (3–1100  $\mu\text{m}$ ) and  $C = 41.27$  for  $H\alpha$  ([Hao et al. 2011](#); [Murphy et al. 2011](#)), we obtain the expected relation for star-forming galaxies of:

$$\log_{10}(L_{\text{TIR}}) = \log_{10}(L_{H\alpha}) + 2.14. \quad (3)$$

We note that these conversions have a number of assumptions underlying them, most notably of constant SFR for 10 Myr for  $L_{H\alpha}$  and 100 Myr for  $L_{\text{TIR}}$ . We will discuss the implications of this approximation at length in Section 5.

*MAGPHYS fitting:* Although the MAGPHYS catalogue was computed by the GAMA team and made available as part of their data release, it is important to understand the underlying dust emission model in order to interpret our results. MAGPHYS is an energy balance code that assumes that all stellar light absorbed from the UV–optical wavelength range is re-emitted in the mid- and far-IR. It fits a two component dust emission model, with one contribution from dust in the stellar birth clouds, and the second from dust in the ambient ISM (see figure 2 in [da Cunha et al. 2008](#)). Both components contribute to flux emitted by polycyclic aromatic hydrocarbons (PAHs) and hot mid-IR continuum. The

birth clouds additionally contribute warm dust in thermal equilibrium, while the ambient ISM contributes cold thermal dust. Free parameters are the fraction of total IR luminosity contributed by dust in the ambient ISM, the temperature of the two thermal components, and relative fractions of light contributed by the different birth cloud components.

We note that the total IR luminosity output by MAGPHYS is calculated from the energy lost in the UV–optical wavelength regime, which is then distributed via the model between 3–1000  $\mu\text{m}$ . Although  $L_{\text{TIR}}$  is necessarily model dependent due to the sparse sampling of the IR SED by observations, comparisons between methods indicate that this does not introduce significant errors (e.g. [Hunt et al. 2019](#)).

*Modified black body fitting:* To ensure that our results are not dependent on the MAGPHYS model, we independently fit the total IR luminosity with a modified black body, using the python MCMC package *emcee* ([Foreman-Mackey et al. 2013](#)). We assume a fixed dust emissivity index  $\beta = 1.8$  and a dust mass absorption coefficient  $\kappa_{850} = 0.077 \text{ m}^2 \text{ kg}^{-1}$  and include a mid-infrared power-law to account for hot dust, allowed to vary uniformly between  $0.5 < \alpha < 5.5$  (see also [Casey 2012](#); [Bourne et al. 2019](#)). We fit for a temperature range between 10 and 100 K using a uniform prior. We obtain a very tight 1:1 correlation between our measurement of  $L_{\text{TIR}}$  and the value from MAGPHYS, with a Spearman rank correlation coefficient of 0.99 when all 6 mid- to far-IR bands are detected at  $> 3\sigma$ , decreasing slightly to 0.96 when only 3 bands are detected.

*Aperture correction:* Finally, our  $L_{H\alpha}$  values are measured within a  $3''$  diameter aperture fibre, with atmospheric seeing further scattering the light beyond the fibre aperture. On the other hand the MAGPHYS  $L_{\text{TIR}}$

values are measured from the global galaxy photometry. For our sample of 4,121 galaxies, the median amount of  $z$ -band light contained within the fibre is 0.27, with 16th and 84th percentiles of 0.18 and 0.37. This effect can be approximately corrected by dividing the spectral flux by the fraction of  $z$ -band light ( $L_z$ ) contained within the fibre. This will be less accurate in the case of strong radial gradients in  $L_{H\alpha}/L_z$ , however we checked that there were no redshift trends in any of our results which would suggest this to be a problem. We initially performed our analysis with  $L_{H\alpha}$  values uncorrected for this aperture effect, and the results were qualitatively identical. The advantage of doing the aperture correction explicitly is that galaxies with differing surface brightness profiles are treated properly relative to one another. The fact that our final  $L_{TIR}/L_{H\alpha}$  ratio for highly star-forming galaxies lines up so well with that expected in the literature, and there are no redshift trends in our results, gives confidence that this method is appropriate.

#### 4. RESULTS

The left panel of Figure 2 presents the total dust luminosity ( $L_{TIR}$ ), as estimated by MAGPHYS between 3–1000  $\mu\text{m}$ , versus the dust and aperture corrected  $H\alpha$  luminosity ( $L_{H\alpha}$ ) for all galaxies in our sample, colour coded by the equivalent width of  $H\alpha$  ( $W_{H\alpha}$ ). We plot  $W_{H\alpha}$  as this is a direct observable; for galaxies with emission lines dominated by star formation  $W_{H\alpha}$  is strongly correlated with specific SFR ( $\text{sSFR} = \text{SFR}/M_*$ ). If both  $L_{H\alpha}$  and  $L_{TIR}$  were tracing SFR, galaxies should lie on the blue line. We can immediately see that this is only true for galaxies with  $W_{H\alpha} \gtrsim 10\text{\AA}$ . Retired galaxies with  $W_{H\alpha} \lesssim 3\text{\AA}$  (yellow to red points), lie significantly above or to the left of the line, with higher  $L_{TIR}$  than expected for their  $L_{H\alpha}$ . This can not be explained by contamination of the  $H\alpha$  line by additional ionisation sources such as AGN, HOLMES or shocks, as such contamination would scatter galaxies to the right of the blue line. The arrow indicates the direction of partial correlation ( $\theta_p = -55^\circ$ ), confirming  $W_{H\alpha}$  to be strongly positively correlated with  $L_{H\alpha}$ , and negatively with  $L_{TIR}$ .

The right hand panel of Figure 2 restricts the sample to the 1,638 galaxies with optical emission line ratios that indicate the gas is predominantly ionised by young stellar populations and therefore  $L_{H\alpha}$  is a good proxy for SFR (Section 2.1.1). It is noteworthy that there is still a trend with  $W_{H\alpha}$ , with the conversion line equating both luminosities to SFR only holding for galaxies with  $W_{H\alpha} \gtrsim 10\text{\AA}$  (Hao et al. 2011; Murphy et al. 2011; Kennicutt & Evans 2012). All other galaxies with lower  $W_{H\alpha}$  lie above the line, with higher  $L_{TIR}$  than expected for their  $L_{H\alpha}$ . The partial correlation angle of  $\theta_p = -48^\circ$  indicates that  $W_{H\alpha}$  traces  $L_{TIR}$  just as much as it does  $L_{H\alpha}$  and we can see that *accounting for  $W_{H\alpha}$  would account for most of the scatter in the relation*. The results shown in these figures are unchanged if we use a simple modified black body fit to the mid- and far-infrared data (see Section 3).

In both panels of Figure 2 the post-starburst galaxies are indicated by larger circles. The identical colour scaling of the post-starburst galaxies relative to the background population of galaxies demonstrates that post-starburst galaxies are not unusual in their dust luminosities, given their  $H\alpha$  equivalent widths. The majority of the post-starburst galaxies lie above the star-forming sequence in  $L_{TIR}$  versus  $L_{H\alpha}$ . The small number with  $W_{H\alpha} \lesssim 3\text{\AA}$  have the highest excess  $L_{TIR}$ .

Our results show that all post-starburst galaxies have dust luminosities larger than predicted by  $L_{H\alpha}$ , but consistent with star-forming galaxies or retired galaxies with the same  $W_{H\alpha}$ . If these post-starburst galaxies are in fact ‘dust obscured starbursts’, then the excess  $L_{TIR}$  common to *all galaxies* with  $W_{H\alpha} < 10\text{\AA}$  should be interpreted as due to complete obscuration of the  $H\alpha$  line. In Section 5 we will discuss why we do not think this is the case.

To further investigate the cause of the varying  $L_{TIR}/L_{H\alpha}$  ratio with  $W_{H\alpha}$ , Figure 3 shows the same samples plotted as stellar mass  $M_*$  versus  $L_{H\alpha}$ . We overplot lines of constant sSFR, although caution that these are only relevant where  $L_{H\alpha}$  arises predominantly from star formation. The top left panel largely repeats the information presented in Figure 2, but the inclusion of stellar mass makes the blue and red sequences stand out more clearly. Interestingly, the  $L_{TIR}/L_{H\alpha}$  ratio changes smoothly across this figure, with no obvious discontinuity between the blue and red sequences, or for the post-starburst galaxies. The partial correlation angle of  $\theta_p = -38^\circ$  is consistent with  $L_{TIR}/L_{H\alpha}$  trending most closely with  $L_{H\alpha}/M_*$  (or sSFR for galaxies where  $L_{H\alpha}$  is dominated by star-formation). The smoothness of the transition suggests that *whatever is responsible for the varying ratio has no knowledge of the origin of the emission, or whether the galaxy is quenched, recently quenched or still star-forming*.

Red sequence galaxies clearly have the highest  $L_{TIR}/L_{H\alpha}$ , with the majority having a ratio more than 1 dex greater than the expected ratio based on standard conversions (2.14, see Section 3), while 19 galaxies have a ratio  $\geq 1.5$  dex greater. If we accounted for contamination of the  $H\alpha$  line from ionisation sources that are not related to star formation, such as AGN, shocks or HOLMES, this discrepancy would further increase. At the other extreme, galaxies with either very high  $L_{H\alpha}/M_*$  (high sSFR for galaxies where  $L_{H\alpha}$  is dominated by star-formation) or very high  $L_{H\alpha}$  have a ratio that is lower than expected, with 32 having a ratio  $\geq 0.5$  dex lower. Again we see that post-starburst galaxies, whether completely quenched or not, have the expected  $L_{TIR}/L_{H\alpha}$  ratio compared to other galaxies with the same stellar mass and  $L_{H\alpha}$ .

The top right panel colours the galaxies by  $L_{TIR}$ . This visualisation adds no new data, but again demonstrates the continuity between the blue and red sequence.  $L_{TIR}$  depends almost equally on  $L_{H\alpha}$  and  $M_*$ , i.e. at fixed  $L_{H\alpha}$ ,  $L_{TIR}$  increases with  $M_*$ , again showing that both

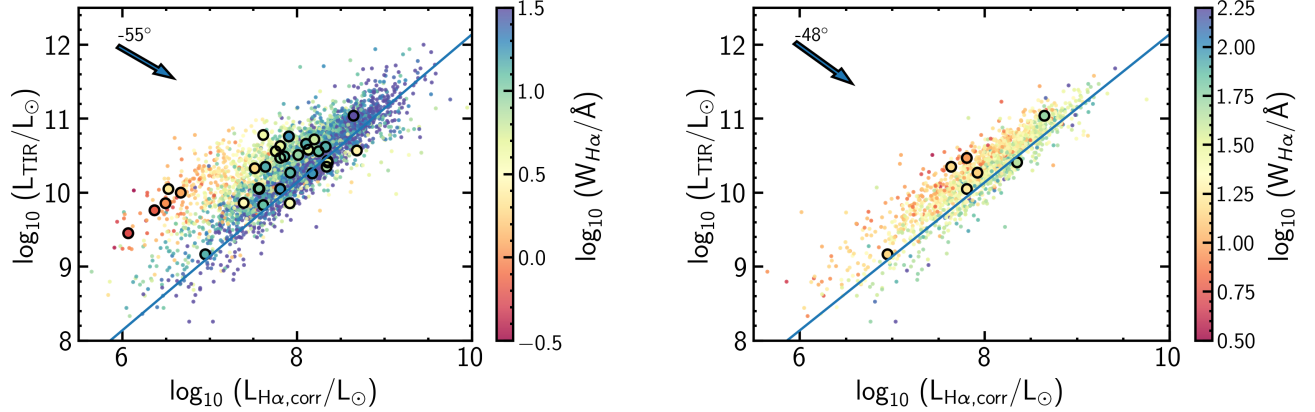


**Figure 2.** The total dust (mid-far infrared) luminosity versus  $H\alpha$  luminosity for galaxies observed in both SDSS and GAMA/Herschel-ATLAS/WISE (small dots), where  $L_{H\alpha}$  has been both dust and aperture corrected. Post-starburst galaxies are shown as large circles with the same colour scale. We only include galaxies with  $H\alpha$  flux detected at  $> 5\sigma$  and fluxes in 2 or more 22–500  $\mu\text{m}$  bands detected at  $> 3\sigma$ . The arrow and angle indicate the direction of partial correlation with the  $z$  (colour) axis. The line indicates equity in the case that both luminosities trace the galaxy SFR, assuming standard conversions from the literature. No smoothing has been applied to the data. *Left:* all galaxies, regardless of the origin of the  $H\alpha$  flux. *Right:* only galaxies where the  $H\alpha$  flux comes predominantly from star-formation, as determined from their emission line ratios (see text for details).

quantities cannot trace SFR. The smoothness of the colour scaling across the blue and red sequence again shows that  $L_{\text{TIR}}$  is entirely agnostic as to the origin of the emission or quenched status of the galaxy.

The lower left panel colours the galaxies by the fraction of total dust luminosity that is fit by the ambient ISM dust component in MAGPHYS ( $f_{\mu,\text{IR}}$ ), as opposed to the birth cloud dust surrounding the star-forming regions. We note that this result is dependent on the MAGPHYS model, unlike previous results, but is useful to further interpret our results. Here we see a more distinct discontinuity between the blue and red sequences, with the majority of red sequence galaxies requiring  $\lesssim 10\%$  additional contribution from a hotter birth cloud component, while the blue sequence galaxies have typically  $\gtrsim 50\%$  contribution from hotter birth clouds.

The lower right panel colours the galaxies by the temperature of the ambient ISM dust component fit by MAGPHYS. Constraining dust temperature accurately requires more dust bands than a simple dust luminosity, we therefore required galaxies to be detected at  $5\sigma$  in 3 or more 22–500  $\mu\text{m}$  bands for this analysis (2,877 galaxies)<sup>4</sup>. While there is a significant scatter, the predominant trend is for galaxies with higher  $L_{H\alpha}$  to have higher temperature ISM dust ( $\theta_p = -15^\circ$ ). There is a small residual trend with stellar mass, but not to the same extent as for  $L_{\text{TIR}}/L_{H\alpha}$ . This shows that the changing ISM dust temperature is not the cause of the changing luminosity ratio. MAGPHYS also fits for the temperature of the birth cloud thermal component (not shown). We find a similar result, with galaxies with higher  $L_{H\alpha}$  having higher temperature birth cloud dust and any residual trend with stellar mass being small.

<sup>4</sup> For both the bottom left and bottom right panels, we verified that the results do not change if we require significant detections in more mid and far-IR bands.

We investigated various other correlations in the dataset, which are not shown for conciseness, but we describe a couple more here. Dust attenuation, as measured by both the emission line Balmer decrement and by the MAGPHYS multi-wavelength photometric fit, follows the same trend as  $L_{\text{TIR}}$  in blue sequence galaxies i.e. higher mass, higher  $L_{H\alpha}$  galaxies have greater attenuation. However, the trend does not extend to the red sequence, where there is lower attenuation overall ( $\tau_{V,\text{Balmer}} \lesssim 0.5$ ). The relative luminosity fraction of the warm and cold thermal components fit by MAGPHYS are correlated predominantly with stellar mass, with a small residual trend with  $L_{H\alpha}$ . High mass galaxies and red sequence galaxies have significantly higher fraction of dust fit with a cold thermal component than lower mass, blue sequence galaxies. This provides a consistent picture to that shown for  $f_{\mu,\text{IR}}$ , indicating ambient ISM dust heating depends on stellar mass via the amount of UV and optical photons available from lower mass stars, and therefore contributes most significantly to  $L_{\text{TIR}}$  in red sequence galaxies.

#### 4.1. Post-starburst galaxies

In the above figures it is tempting to look for indications that post-starburst galaxies might have different dust emission properties from the background galaxy population. Such a result might be expected given the commonly assumed origin for post-starburst galaxies as arising from merger induced intense centralised starbursts (although this origin may depend on sample selection, [Ellison et al. 2024](#)). We tested this by selecting a sample of 10 control galaxies for every post-starburst galaxy, matching with the closest Euclidean distance in  $M_*$  and  $L_{H\alpha}$ . We then plotted the distributions of the parameters described in this section, and computed a Kolmogorov–Smirnov test statistic to search for statistically significant differences. Only the contin-



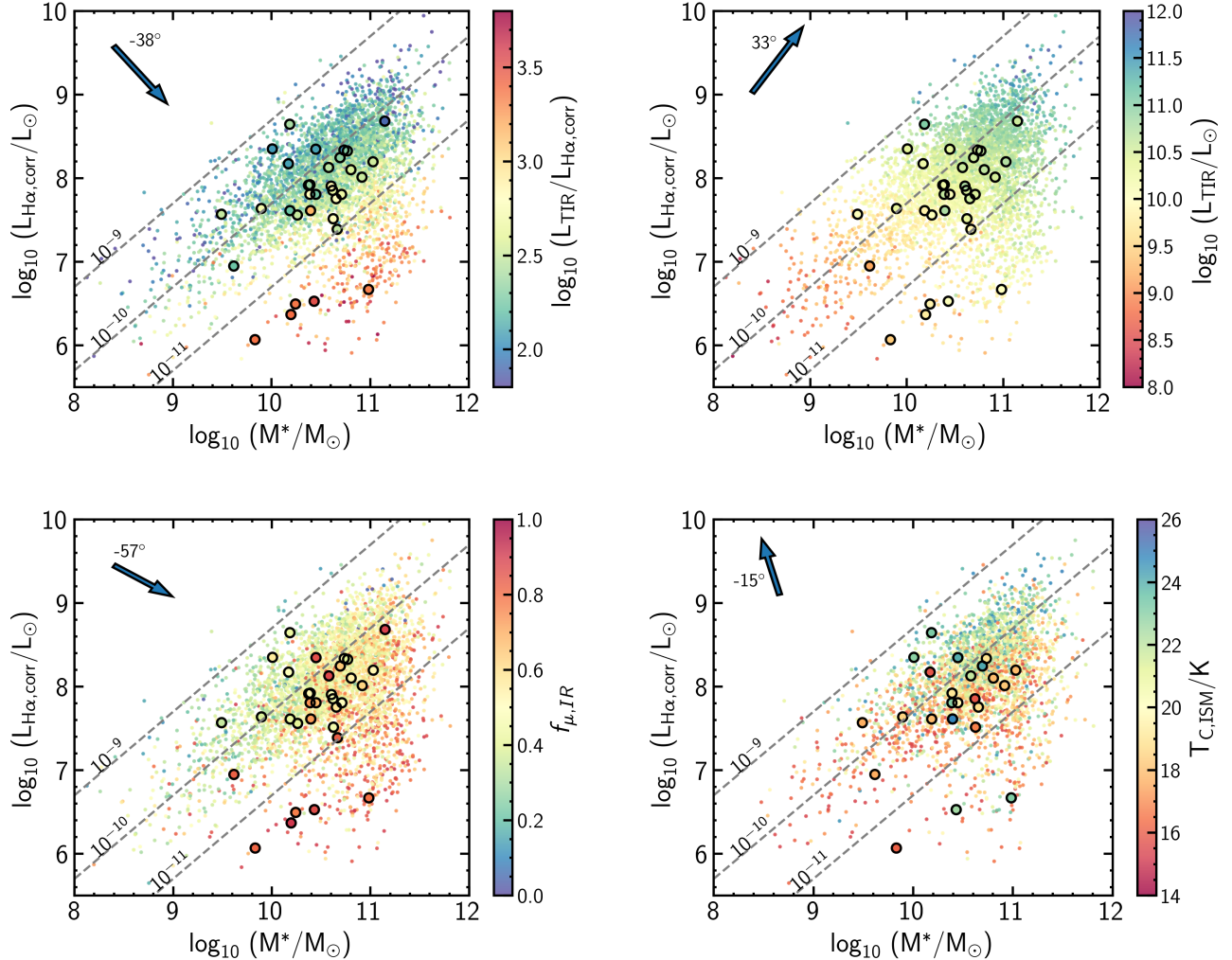


**Figure 3.** Total galaxy stellar mass versus  $H\alpha$  luminosity for the same galaxy samples as in Figure 2.  $H\alpha$  luminosity has been corrected for dust attenuation and aperture, as described in the text. Dashed lines indicate constant sSFR as labelled, in units of  $\text{yr}^{-1}$ . Arrows and angles indicate the direction of partial correlation with the  $z$ -axis quantity. No smoothing has been applied to the data. *Top left:* coloured by total infrared luminosity divided by dust and aperture corrected  $H\alpha$  luminosity. The expected  $\log(\text{ratio})$  is 2.14 based on standard conversions from luminosity to SFR. *Top right:* coloured by total infrared luminosity. *Bottom left:* coloured by fraction of the total dust luminosity coming from the ‘diffuse’ ISM, as fit by MAGPHYS. *Bottom right:* coloured by the temperature of the cool ‘diffuse’ ISM dust component, as fit by MAGPHYS. In this panel we require galaxies to have  $> 5\sigma$  detections in one additional dust band compared to our main analysis.

uum optical depth as measured by MAGPHYS showed a noteworthy, albeit statistically marginal, difference between the post-starburst and control galaxies ( $D = 0.25$ ,  $p\text{-value} = 0.04$ ), with the post-starburst galaxies having a slightly higher median value of  $\tau_V = 1.4$  versus 1.1 for the mass and luminosity matched control sample. *Our results conclusively show that there is no substantial difference in either the dust luminosity, or the dust properties, of post-starburst galaxies compared to galaxies with more normal star formation histories matched in  $M_*$  and  $L_{H\alpha}$ .*

## 5. DISCUSSION

There are two scenarios by which  $L_{\text{TIR}}$  and  $L_{H\alpha}$  should not track each other, which are interrelated, yet subtly different. Firstly, dust heating of older stars contributes more to  $L_{\text{TIR}}$  than to  $L_{H\alpha}$ . The extent to which this

matters depends on (a) the mass of older stars in the galaxy, and therefore on the star formation history of the galaxy in the distant past, and (b) the presence of ambient ISM that is available to be heated. Secondly, even in a star-forming galaxy, if the SFR rapidly decreases,  $L_{H\alpha}$  will decrease rapidly while  $L_{\text{TIR}}$  will remain high for  $\sim 100$  Myr. In this section we argue that dust heating by older stars, rather than a recent change in SFR, is the dominant effect.

### 5.1. A two-component ISM

In the standard picture (e.g. [Helou 1986](#); [Lonsdale Persson & Helou 1987](#); [Draine & Li 2007](#)), a galaxy ISM contains a temporally stable ambient reservoir of dust that is built up steadily via many generations of stars. Alongside this ambient dust, there are temporally tran-

sient dense birth clouds surrounding new star-forming regions; the greater the number of star-forming regions, the greater the number of dense birth clouds. When these young star-forming regions dominate over the ambient dust, we find that  $L_{\text{TIR}}$  correlates strongly with  $L_{\text{H}\alpha}$  and both provide a good estimate of SFR in galaxies. As the specific SFR of the galaxy declines,  $L_{\text{TIR}}$  becomes increasingly dominated by the ambient dust. This standard picture of dust in galaxies is the basis of the two component dust model of [Charlot & Fall \(2000\)](#), which is the model implemented in MAGPHYS, as well as some other SED modelling codes (e.g. GRASIL, [Domínguez-Tenreiro et al. 2014](#)).

In fact, the sources of  $L_{\text{H}\alpha}$  in galaxies can be thought of in much the same way as the sources of  $L_{\text{TIR}}$ : a background population of hot, low mass, evolved stars (HOLMES) provides the temporally stable equivalent of the ambient dust that builds up over time, while the temporally transient hot OB stars provide the majority source of Lyman continuum photons when present. Not entirely coincidentally of course, the timescale during which we expect OB stars to stop providing Lyman continuum photons is of the same magnitude as the timescale that we expect the dense birth clouds to disperse. Therefore, as sSFR decreases, the stellar population moves from OB star dominated to G+ star dominated, at the same rate that the dust clouds move from birth cloud dominated to diffuse ISM dominated.

However,  $L_{\text{TIR}}$  and  $L_{\text{H}\alpha}$  respond differently to the stellar population mix. Because  $L_{\text{H}\alpha}$  emission caused by HOLMES is very weak,  $L_{\text{H}\alpha}$  drops very sharply once the star-forming regions vanishes. On the other hand,  $L_{\text{TIR}}$  drops more slowly over a time period of 100 Myr, and remains persistently higher than  $L_{\text{H}\alpha}$  until the dust is destroyed, because dust can be heated by all stars emitting in the UV and optical wavelength regime (see figure 3 of [Hayward et al. 2014](#)). Thus, the  $L_{\text{TIR}}/L_{\text{H}\alpha}$  ratio increases and remains high after a decline in star formation, reflecting the higher fraction of dust luminosity coming from the ambient ISM compared to the fraction of  $L_{\text{H}\alpha}$  coming from older stars. We hypothesise that it is this effect that causes the smooth trend between  $L_{\text{TIR}}$ ,  $L_{\text{H}\alpha}$  and  $M_*$  continuing into the red sequence, without discontinuity, despite the apparently different ionising and heating mechanisms, and star formation histories of the galaxies. The changing  $L_{\text{TIR}}/L_{\text{H}\alpha}$  with  $L_{\text{H}\alpha}/M_*$  then simply reflects the differing relative importance of OB stars to HOLMES for  $L_{\text{H}\alpha}$ , and diffuse ISM to birth clouds for  $L_{\text{TIR}}$  emission.

As discussed in Section 3, when luminosities are converted into a SFR, a constant SFR over a fixed timescale is assumed (10 Myr for  $L_{\text{H}\alpha}$  and 100 Myr for  $L_{\text{TIR}}$ ). While this might be a reasonable approximation for a star-forming galaxy, it clearly is not for a young post-starburst galaxy where the SFR has dropped precipitously over the past hundred Myr. To untangle the relative importance of star formation history versus ambient dust heating to the excess  $L_{\text{TIR}}$  seen in retired, post-

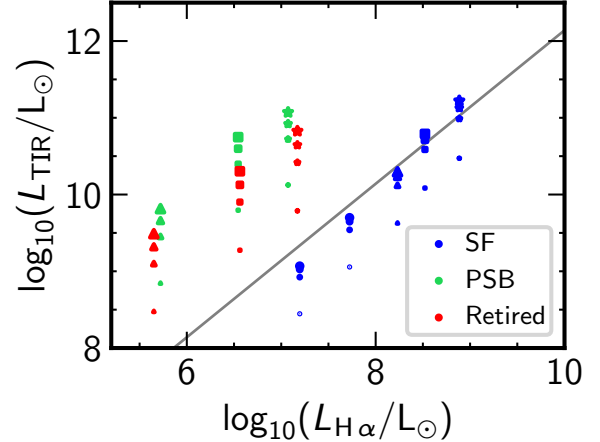


**Figure 4.** Total infrared versus  $\text{H}\alpha$  luminosity for the star-forming (SF), post-starburst (PSB) and retired toy models in  $M_*$  bins. Triangles, squares and stars are used respectively for the middle, second-to-last and largest mass bins. The two lowest-mass bins for star-forming galaxies are shown as dots. Larger symbols indicate larger effective dust attenuation, with  $\tau_V = 0.1, 0.5, 1.0$  and  $2.0$ . The grey line is the SFR conversion line as in Figure 2.

starburst and star-forming galaxies with  $W_{\text{H}\alpha} < 10 \text{ \AA}$ , we turn to toy models.

## 5.2. Toy SED models

To illustrate how  $L_{\text{H}\alpha}$  and  $L_{\text{TIR}}$  depend on a galaxy’s stellar populations, we constructed a set of toy SED models based on average star formation histories for star-forming, post-starburst and retired galaxies in the STARLIGHT–SDSS main galaxy sample catalogue. We note that the post-starburst galaxies were selected via the [Goto \(2007\)](#) method, meaning they have completely ceased star-formation and thus match the subset of our post-starburst galaxies with  $W_{\text{H}\alpha} < 3 \text{ \AA}$ . The models were constructed in mass bins of 1 dex using [Bruzual & Charlot \(2003\)](#) models with a [Chabrier \(2003\)](#) initial mass function. Further details are provided in Appendix A, including a figure demonstrating the difference in star formation histories between the star-forming, retired and post-starburst samples (Figure A1).

We calculated  $L_{\text{H}\alpha}$  from the extrapolated SED models in the UV by integrating the rate of ionizing photons, assuming the case B hydrogen recombination and an ionisation-bounded scenario (as in [Stasińska et al. 2006](#); [Cid Fernandes et al. 2011](#)). For quenched post-starburst and retired galaxies, since the measured light fraction from young stars is over-estimated due to limitations in the stellar population models, we only considered stellar populations older than  $10^8 \text{ yr}$  (see [Ocvirk 2010](#); [Cid Fernandes et al. 2011](#), equation 2 and footnote 6).

From the intrinsic model spectrum  $L_{\lambda}^{\text{int}}$ , we modelled a dust reddened spectrum assuming a single dust screen,

$$L_{\lambda}^{\text{obs}} = L_{\lambda}^{\text{int}} e^{-\tau_V q_{\lambda}}, \quad (4)$$

where  $\tau_V$  is the effective dust attenuation in the V-band and  $q_{\lambda} \equiv \tau_{\lambda}/\tau_V$  is the shape of the dust attenuation law, here taken to be the [Cardelli et al. \(1989\)](#) extinc-

tion curve with  $R_V = 3.1$ . We created models with four values of the effective dust attenuation,  $\tau_V = 0.1, 0.5, 1.0$  and  $2.0$ .  $L_{\text{TIR}}$  was then calculated by integrating the difference between the intrinsic and dust reddened spectrum, and assuming all light attenuated by dust is re-radiated in the mid- and far-IR.

Figure 4 shows the results of our toy models in the  $L_{\text{H}\alpha}$ – $L_{\text{TIR}}$  plane, which closely match those seen in Figure 2. Larger symbol sizes indicate greater  $\tau_V$  values, which affect only  $L_{\text{TIR}}$ , since the intrinsic and dust-corrected  $L_{\text{H}\alpha}$  are taken to be the same. Triangles, squares and stars are used respectively for the middle, second-to-last and largest mass bins. *Crucially, only models for star-forming galaxies fall onto the SFR conversion line, with retired and quenched post-starbursts lying up to 1.5 dex above it, supporting our conclusion that  $L_{\text{TIR}}$  is only suitable as an SFR indicator in galaxies that are actively star forming.*

When going from models for star-forming galaxies to post-starburst/retired galaxies, within the same mass and  $\tau_V$  bin (fixed symbol style and size, changing colour) there is a slight decrease in  $L_{\text{TIR}}$  as old stars still heat the diffuse ISM, and a huge drop in  $L_{\text{H}\alpha}$ . This highlights the fact that HOLMES are a much less powerful ionising source than OB stars: the rate of ionising photons decreases by five orders of magnitude from a 10 Myr to a 1–10 Gyr stellar population (see figure 1, panel b of Cid Fernandes et al. 2011).

The slightly higher  $L_{\text{TIR}}$  of the quenched post-starburst galaxies compared to retired galaxies is due to the presence of a large number of relatively hot A and F stars to heat the dust, rather than the recent precipitous drop in SFR (which from Figure A1 can be seen to be insignificant for well over the 100 Myr averaging time assumed for  $L_{\text{TIR}}$  in star-forming galaxies). The comparatively small difference between post-starburst and retired galaxies, compared to the difference between post-starburst and star-forming galaxies, shows that *the recent star formation history is a much less important factor than the specific star formation rate in determining the  $L_{\text{TIR}}/L_{\text{H}\alpha}$  ratio.*

Our toy models do not include post-starburst galaxies that are in the process of quenching, which are seen in Figure 2 to lie just above the star-forming sequence. Here we expect a combination of a rapidly declining recent SFR and a reduction in birth cloud dust to be contributing to the enhanced  $L_{\text{TIR}}$  compared to  $L_{\text{H}\alpha}$  (see also Hayward et al. 2014). We also do not include any timescale for dust destruction, so our toy models are only pertinent to galaxies which have some ambient ISM available to be heated.

### 5.3. Dust-star geometry, interstellar radiation field, dust destruction and cloud density

Interestingly, the many complications that could arise in terms of dust temperature, dust-star geometry, dust destruction and dust cloud density and even ionisation source do not appear to be important to our results, at

least to first order, even for post-starburst galaxies which should provide a test of the most extreme quenching conditions. At far-IR wavelengths, the temperature of the dust is thought to be determined mostly by the dust-star geometry, rather than the shape of the interstellar radiation field (ISRF, e.g. Bernard et al. 2010). Thus, for any given stellar population mix, the stars which emit the most UV–optical photons will contribute most to the total  $L_{\text{TIR}}$ , i.e. OB stars in star-forming galaxies, AF stars in post-starburst galaxies, or G and later in retired galaxies, but the differing temperature of the stars is not relevant. The MAGPHYS SED modelling results shown in Figure 3 suggest that dust temperature correlates most strongly with  $L_{\text{H}\alpha}$ , with a small residual mass trend. MAGPHYS modelling also suggests that galaxies with the highest  $L_{\text{H}\alpha}$  in our sample have higher ambient ISM and dense birth cloud dust temperatures. This is expected to be due to the closer proximity of the dust to the star-forming regions, rather than the changing ISRF (e.g. Nersesian et al. 2019). These particular results will likely be sensitive to the assumed model, and deserve further exploration.

The lack of any appreciable difference in the temperature of post-starburst galaxy ISM dust compared to normal galaxies is interesting (bottom right panel of Figure 3), as we might expect the A/F stars to be co-located with the majority of the ISM dust following the end of the starburst, and therefore able to enhance the heating in a similar way to the brightest starbursts. Rowlands et al. (2015) found a decrease in post-starburst dust temperature with time since burst. However, they were studying generally younger post-starburst galaxies than in this sample, and temperature was estimated from colour index rather than the MAGPHYS fit as used here. It seems likely that the dust heating observed in the youngest post-starbursts in their sample was due to a changing balance of hot birth cloud dust to cooler ISM dust following the star-formation episode, rather than a more general heating of the ambient ISM i.e. closer to the  $f_{\mu\text{IR}}$  parameter in the bottom left panel of Figure 3. Over time and with no subsequent star formation we expect the dust to be destroyed, and here post-starburst galaxies provide a valuable timescale that can be used to constrain the mechanisms responsible for dust destruction. Li et al. (2019) used the unique clock provided by post-starburst galaxies to measure a timescale for dust destruction of  $\sim 250$  Myr. By 1 Gyr post-burst, the majority of post-starburst galaxies have no detectable dust.

### 5.4. SFR estimators and full spectral fitting

The debate about the importance, or otherwise, of dust heating by lower mass stars has a long history, with both sides likely ‘right’ in their context. In early works, the inability to correct  $L_{\text{H}\alpha}$  for stellar absorption and dust attenuation led to the conclusion that IR was a better total SFR indicator for galaxies, regardless of what was heating it (e.g. Lonsdale & Helou 1985). However, this argument became obsolete once better optical data be-

came available (e.g. Rosa-González et al. 2002; Kewley et al. 2002) and the two were shown to be exceedingly tightly correlated in local star-forming galaxies.

Another argument is that it does not matter where the photons come from, they still represent star formation, and should be counted even if the star formation happened long ago. This is because combining  $L_{\text{TIR}}$  with a UV luminosity to account for the unextincted photons accounts for most photons generated by stars that are still alive at the time of observation, regardless of their mass or when they were formed. However, this argument is only plausibly useful when integrating in both time and space, not when trying to estimate the ongoing SFR of a particular galaxy, or set of galaxies, as it does not tell us the number of stars recently formed.

A more important, yet subtle, discussion is around the timescales for different SFR estimators. To obtain the current SFR of a galaxy, the basic underlying principle is to count the number of stars just formed. This is, however, not easy for spatially unresolved data – in reality we have to count the brightest, and therefore hottest, stars formed, then assume an initial mass function to give us the SFR. Unfortunately, even this is hard to do, so we resort to proxy estimators that are necessarily time averaged.

For  $L_{\text{H}\alpha}$  the time-averaging is the main sequence lifetime of O and B stars, about 10 Myr. It is this short timescale that makes it attractive as a robust SFR indicator. For FIR, the time averaging is around 100 Myr for star-forming galaxies, which accounts for lower mass stars also heating the dust (Kennicutt 1998). All conversions between a proxy luminosity and SFR require the assumption of a constant SFR over the averaging timeframe. For some galaxies, such as those which are currently rapidly declining in SFR, the longer estimators may be less suitable. Our results, supplemented by our toy models, highlight the subtle difference between star formation history versus contamination by ambient ISM dust in enhancing  $L_{\text{TIR}}/L_{\text{H}\alpha}$ . The post-starburst galaxies in our sample that are currently decreasing in SFR, but still have appreciable SFR, have a slightly enhanced  $L_{\text{TIR}}$  for their  $L_{\text{H}\alpha}$ , and they lie close to ordinary star-forming galaxies. This could be due to their rapidly declining star formation history, as well as their reducing contribution of birth cloud dust to  $L_{\text{TIR}}$ . On the other hand, the post-starburst galaxies that have completely quenched their SFR have a very substantially enhanced  $L_{\text{TIR}}$  for their  $L_{\text{H}\alpha}$ , causing them to lie close to the retired galaxies. When the observed luminosity is dominated by photons from significantly lower mass stellar populations, we are no longer measuring the number of recently formed stars, but rather the integrated mass formed during the entire lifetime of the galaxy. This leads to a strong correlation between  $L_{\text{TIR}}$  and  $M_*$ , rather than  $L_{\text{TIR}}$  and SFR. This suggests that we should see different partial correlation angles between  $L_{\text{TIR}}$ ,  $M_*$  and  $L_{\text{H}\alpha}$  for star-forming, retired and post-starburst galaxies. Unfortunately the small numbers of retired and post-starburst

galaxies in our samples made it impossible to tease these relations apart, and a larger set of retired and quenched post-starburst galaxies would be required.

In principle, obtaining an SFR from full multi-wavelength SED fitting, rather than simple proxy estimators, should solve these problems (Hunt et al. 2019). However, this requires the underlying modelling assumptions to represent reality, both in terms of the star formation histories and the dust emission models. Hunt et al. (2019) shows that different SED fitting models and proxy indicators disagree the most when sSFR is low, suggesting that not all SED fitting models include the correct assumptions (or model ‘priors’) in this regime.

### 5.5. Comparison to previous work

It has long been known that dust heating by old stars will impact low sSFR galaxies more than their high sSFR counterparts, with many cautionary notes in the literature (see e.g. Kennicutt 1998). In this section we compare our results to previous studies where mid- and far-IR luminosities have been noticed to apparently overestimate SFR in galaxies.

Although papers purposefully studying SFR calibrators commonly investigate galaxy types, few provide measurements of the  $W_{\text{H}\alpha}$  or sSFR of the galaxies being used for calibration. One exception is Hao et al. (2011) where the majority of galaxies have  $W_{\text{H}\alpha} > 10 \text{ \AA}$ , and their figure 7 shows an overestimation of the SFR using an FIR-based calibrator by 0.3 dex for the small number of galaxies with  $W_{\text{H}\alpha} > 5 \text{ \AA}$ . This is entirely consistent with our results.

Salim et al. (2016) presented the GALEX-SDSS-WISE Legacy catalogue, noting that galaxies with  $\log_{10}(\text{sSFR}/\text{yr}^{-1}) < -11$  have mid-IR SFRs biased high by up to 2 dex, attributing this to the dust being heated primarily by old stars. Similarly, Rosario et al. (2016) looked at  $L_{\text{H}\alpha}$  versus  $L_{\text{TIR}}$  in an early Herschel-SDSS sample similar to that studied here, and while they did not link their results to star formation histories, their plots show the same excess of  $L_{\text{TIR}}$  in low sSFR galaxies. Kouroumpatzakis et al. (2023) used the SED modelling code CIGALE (Boquien et al. 2019) to show that mid-IR-based SFR estimators overpredict SFR compared to CIGALE for galaxies with  $W_{\text{H}\alpha} < 10 \text{ \AA}$ . It is reassuring that entirely different analyses have lead to the same quantitative results.

Our results are also consistent with those of Nersesian et al. (2019) who used CIGALE to note that galaxies with  $\log_{10}(\text{sSFR}/\text{yr}^{-1}) > -10.5$  had dust mainly heated by radiation emitted by the young population, whereas lower sSFR galaxies had dust heated by the older population. This corresponds to  $W_{\text{H}\alpha} > 10 \text{ \AA}$ , matching our results. Recently Parente et al. (2024) have used a semi-analytic galaxy evolution model coupled to the GRASIL radiative transfer model to demonstrate the dust content of galaxies transitioning through the green-valley remains high following star formation quenching, leading to relatively large 250  $\mu\text{m}$  fluxes in agreement with



GAMA observations.

And finally, our results are consistent with the spatially resolved PHANGS–MUSE SFR calibration comparisons of Belfiore et al. (2023), who noted a systematic increase in IR-based SFR estimators compared to dust attenuation corrected  $L_{H\alpha}$  at low specific star formation rates of  $\log_{10}(\text{sSFR}/\text{yr}^{-1}) < -10$ .

*All these results show that IR-based SFR indicators should only be used where  $W_{H\alpha} > 10 \text{ \AA}$  or  $\log_{10}(\text{sSFR}/\text{yr}^{-1}) > -10.5$ .*

## 6. SUMMARY

We have compared the  $H\alpha$  luminosity, corrected for dust and aperture effects, to the total IR luminosity of 4,121 galaxies observed in both spectroscopic SDSS DR7 and GAMA DR4 catalogues, with detections in the mid- and far-IR observations from WISE and Herschel–ATLAS. We find that:

- $L_{\text{TIR}}$  is strongly correlated with  $L_{H\alpha}$  for galaxies with  $W_{H\alpha} \gtrsim 10 \text{ \AA}$  or  $\log_{10}(\text{sSFR}/\text{yr}^{-1}) > -10.5$ , with a ratio that is consistent with locally determined calibrations. In this regime, both  $L_{H\alpha}$  and  $L_{\text{TIR}}$  can be used to estimate integrated SFRs of galaxies.
- However, for galaxies with  $W_{H\alpha} \lesssim 10 \text{ \AA}$  or  $\log_{10}(\text{sSFR}/\text{yr}^{-1}) < -10.5$ ,  $L_{\text{TIR}}/L_{H\alpha}$  increases by up to 1.5 dex. In this regime,  $L_{\text{TIR}}$  should not be used to measure the integrated SFRs of galaxies. We remind readers that  $L_{H\alpha}$  can only be used to estimate the SFR of galaxies when  $W_{H\alpha} \gtrsim 3 \text{ \AA}$  (Cid Fernandes et al. 2011).
- The smoothness in the relationships between  $L_{\text{TIR}}$ ,  $L_{H\alpha}$  and galaxy stellar mass for galaxies, regardless of their dominant heating or ionisation source, is consistent with the ‘standard’ 2-component picture for dust emission in galaxies. A background of old, low mass stars both heat the dust and provide a low level background of ionising photons in all galaxies, regardless of sSFR. As sSFR increases, the number of star-forming regions increases, and these then dominate the heating and ionisation budget.
- The reason for the increasing  $L_{\text{TIR}}/L_{H\alpha}$  ratio with decreasing sSFR is simply due to the fact that dust is heated by UV–optical photons, while  $L_{H\alpha}$  relies on Lyman continuum photons alone. Thus,  $L_{H\alpha}$  decays rapidly once star formation ceases with old stars providing only a very small number of far-UV photons, while dust continues to emit, presumably until the grains are destroyed.
- We use toy models to show that the excess  $L_{\text{TIR}}$  is predominantly due to the increasing dominance of old, low mass stars heating the dust, and not due to a recent decline in star formation rate, combined with the assumption of constant star formation rates in the calibration conversions of luminosity

into SFR. However, the rare population of galaxies with ongoing, yet rapidly declining, star formation rates (young post-starburst galaxies) may have slightly enhanced  $L_{\text{TIR}}$  simply due to the longer averaging time of  $L_{\text{TIR}}$  than  $L_{H\alpha}$  when converted into an SFR.

- Recently and rapidly quenched local post-starburst galaxies do not show any evidence of hosting dust-obscured starbursts. Their high  $L_{\text{TIR}}/L_{H\alpha}$  ratios are entirely consistent with being caused by the above processes.

An improved understanding of heating, ionisation and dust destruction mechanisms in retired and post-starburst galaxies could be gained from spatially resolved observations, both in the mid- and far-IR and with optical integral field spectroscopy. Sensitive radio observations would also provide additional assurance that significant amounts of dust obscured star formation was not being missed from the optical census of the Universe. However, our results indicate that the high fraction of rapidly quenched galaxies detected in optical surveys is not a result of high levels of contamination from dust-obscured starbursts, and therefore understanding rapid quenching pathways to quiescence remains of strong importance to understanding galaxy evolution.

## DATA AVAILABILITY

The SDSS DR7 data is available from <http://classic.sdss.org/dr7/>. The GAMA DR4 catalogues are available from <https://www.gama-survey.org>. STARLIGHT catalogues are available on request to NVA or VW.

## ACKNOWLEDGEMENTS

We would like to thank Rob Kennicutt and Desika Narayanan for their help and advice in interpreting the results, and Kenneth Duncan, Ho-Seong Hwang and Leah Morabito for sharing data and information on datasets during preliminary investigations carried out prior to this paper being written. We would also like to thank Ian Smail and the anonymous OJap referees who provided thoughtful and helpful feedback that improved this manuscript.

VW acknowledges Science and Technologies Facilities Council (STFC) grants ST/V000861/1 and ST/Y00275X/1. NVA and VW acknowledge the Royal Society and the Newton Fund via the award of a Royal Society–Newton Advanced Fellowship (grant NAF\R1\180403). NVA acknowledges support from Conselho Nacional de Desenvolvimento Científico e Tecnológico (CNPq). KR acknowledges support from NASA grant 80NSSC23K0495.

GAMA is a joint European–Australasian project based around a spectroscopic campaign using the Anglo–Australian Telescope. The GAMA input catalogue is based on data taken from the Sloan Digital Sky Survey and the UKIRT Infrared Deep Sky Survey. Com-

plementary imaging of the GAMA regions is being obtained by a number of independent survey programmes including GALEX MIS, VST KiDS, VISTA VIKING, WISE, Herschel-ATLAS, GMRT and ASKAP providing UV to radio coverage. GAMA is funded by the STFC (UK), the ARC (Australia), the AAO, and the participating institutions. The GAMA website is <https://www.gama-survey.org/>.

Funding for the Sloan Digital Sky Survey IV has been provided by the Alfred P. Sloan Foundation, the U.S. Department of Energy Office of Science, and the Participating Institutions. SDSS-IV acknowledges support and resources from the Center for High-Performance Computing at the University of Utah. The SDSS web site is [www.sdss.org](http://www.sdss.org).

SDSS-IV is managed by the Astrophysical Research Consortium for the Participating Institutions of the SDSS Collaboration including the Brazilian Participation Group, the Carnegie Institution for Science, Carnegie Mellon University, the Chilean Participation Group, the French Participation Group, Harvard-Smithsonian Center for Astrophysics, Instituto de Astrofísica de Canarias, The Johns Hopkins University, Kavli Institute for the Physics and Mathematics of the Universe (IPMU) / University of Tokyo, Lawrence Berkeley National Laboratory, Leibniz Institut für Astrophysik Potsdam (AIP), Max-Planck-Institut für Astronomie (MPIA Heidelberg), Max-Planck-Institut für Astrophysik (MPA Garching), Max-Planck-Institut für Extraterrestrische Physik (MPE), National Astronomical Observatories of China, New Mexico State University, New York University, University of Notre Dame, Observatório Nacional / MCTI, The Ohio State University, Pennsylvania State University, Shanghai Astronomical Observatory, United Kingdom Participation Group, Universidad Nacional Autónoma de México, University of Arizona, University of Colorado Boulder, University of Oxford, University of Portsmouth, University of Utah, University of Virginia, University of Washington, University of Wisconsin, Vanderbilt University, and Yale University.

## REFERENCES

- Abazajian K. N., et al., 2009, *ApJS*, **182**, 543  
 Alatalo K., et al., 2016, *ApJS*, **224**, 38  
 Asari N. V., Cid Fernandes R., Stasińska G., Torres-Papaqui J. P., Mateus A., Sodré L., Schoenell W., Gomes J. M., 2007, *MNRAS*, **381**, 263  
 Baldwin J. A., Phillips M. M., Terlevich R., 1981, *PASP*, **93**, 5  
 Baron D., Netzer H., Lutz D., Prochaska J. X., Davies R. I., 2022, *MNRAS*, **509**, 4457  
 Belfiore F., et al., 2023, *A&A*, **670**, A67  
 Bendo G. J., et al., 2010, *A&A*, **518**, L65  
 Bernard J. P., et al., 2010, *A&A*, **518**, L88  
 Boquien M., Burgarella D., Roehlly Y., Buat V., Ciesla L., Corre D., Inoue A. K., Salas H., 2019, *A&A*, **622**, A103  
 Bourne N., et al., 2016, *MNRAS*, **462**, 1714  
 Bourne N., Dunlop J. S., Simpson J. M., Rowlands K. E., Geach J. E., McLeod D. J., 2019, *MNRAS*, **482**, 3135  
 Bruzual G., Charlot S., 2003, *MNRAS*, **344**, 1000  
 Calzetti D., 2013, in Falcón-Barroso J., Knapen J. H., eds., *Secular Evolution of Galaxies*. Cambridge University Press, p. 419, doi:10.48550/arXiv.1208.2997  
 Calzetti D., Armus L., Bohlin R. C., Kinney A. L., Koornneef J., Storchi-Bergmann T., 2000, *ApJ*, **533**, 682  
 Cardelli J. A., Clayton G. C., Mathis J. S., 1989, *ApJ*, **345**, 245  
 Casey C. M., 2012, *MNRAS*, **425**, 3094  
 Chabrier G., 2003, *PASP*, **115**, 763  
 Charlot S., Fall S. M., 2000, *ApJ*, **539**, 718  
 Charlot S., Longhetti M., 2001, *MNRAS*, **323**, 887  
 Chen Y.-M., et al., 2019, *MNRAS*, **489**, 5709  
 Cid Fernandes R., Mateus A., Sodré L., Stasińska G., Gomes J. M., 2005, *MNRAS*, **358**, 363  
 Cid Fernandes R., et al., 2009, in *Revista Mexicana de Astronomía y Astrofísica Conference Series*. pp 127–132  
 Cid Fernandes R., Stasińska G., Schlickmann M. S., Mateus A., Vale Asari N., Schoenell W., Sodré L., 2010, *MNRAS*, **403**, 1036  
 Cid Fernandes R., Stasińska G., Mateus A., Vale Asari N., 2011, *MNRAS*, **413**, 1687  
 Cluver M. E., et al., 2014, *ApJ*, **782**, 90  
 Couch W. J., Sharples R. M., 1987, *MNRAS*, **229**, 423  
 Domínguez-Tenreiro R., Obreja A., Granato G. L., Schurer A., Alpresa P., Silva L., Brook C. B., Serna A., 2014, *MNRAS*, **439**, 3868  
 Draine B. T., Li A., 2007, *ApJ*, **657**, 810  
 Dressler A., Gunn J. E., 1983, *ApJ*, **270**, 7  
 Driver S. P., et al., 2016, *MNRAS*, **455**, 3911  
 Driver S. P., et al., 2022, *MNRAS*, **513**, 439  
 Ellison S. L., Ferreira L., Wild V., Wilkinson S., Rowlands K., Patton D. R., 2024, *submitted to OJA*, p. arXiv:2410.06357  
 Flores-Fajardo N., Morisset C., Stasińska G., Binette L., 2011, *MNRAS*, **415**, 2182  
 Foreman-Mackey D., Hogg D. W., Lang D., Goodman J., 2013, *PASP*, **125**, 306  
 Geach J. E., Smail I., Moran S. M., Treu T., Ellis R. S., 2009, *ApJ*, **691**, 783  
 Goto T., 2007, *MNRAS*, **381**, 187  
 Goto T., et al., 2003, *PASJ*, **55**, 771  
 Groves B., Brinchmann J., Walcher C. J., 2012, *MNRAS*, **419**, 1402  
 Hao C.-N., Kennicutt R. C., Johnson B. D., Calzetti D., Dale D. A., Moustakas J., 2011, *ApJ*, **741**, 124  
 Hayward C. C., et al., 2014, *MNRAS*, **445**, 1598  
 Helou G., 1986, *ApJ Let.*, **311**, L33  
 Herpich F., Stasińska G., Mateus A., Vale Asari N., Cid Fernandes R., 2018, *MNRAS*, **481**, 1774  
 Hunt L. K., et al., 2019, *A&A*, **621**, A51  
 Kennicutt Robert C. J., 1998, *ARA&A*, **36**, 189  
 Kennicutt R. C., Evans N. J., 2012, *ARA&A*, **50**, 531  
 Kennicutt R. C., et al., 2011, *PASP*, **123**, 1347  
 Kewley L. J., Dopita M. A., Sutherland R. S., Heisler C. A., Trevena J., 2001, *ApJ*, **556**, 121  
 Kewley L. J., Geller M. J., Jansen R. A., Dopita M. A., 2002, *AJ*, **124**, 3135  
 Kouroumpatzakis K., Zezas A., Kyritsis E., Salim S., Svoboda J., 2023, *A&A*, **673**, A16  
 Li Z., French K. D., Zabludoff A. I., Ho L. C., 2019, *ApJ*, **879**, 131  
 Lonsdale C. J., Helou G., 1985, in *Bulletin of the American Astronomical Society*. p. 612  
 Lonsdale Persson C. J., Helou G., 1987, *ApJ*, **314**, 513  
 López Fernández R., et al., 2018, *A&A*, **615**, A27  
 Mateus A., Sodré L., Cid Fernandes R., Stasińska G., Schoenell W., Gomes J. M., 2006, *MNRAS*, **370**, 721  
 Murphy E. J., et al., 2011, *ApJ*, **737**, 67  
 Nersesian A., et al., 2019, *A&A*, **624**, A80  
 Ocvirk P., 2010, *ApJ*, **709**, 88  
 Paladini R., Montier L., Giard M., Bernard J. P., Dame T. M., Ito S., Macias-Perez J. F., 2007, *A&A*, **465**, 839  
 Parente M., Ragone-Figueroa C., Granato G. L., Silva L., Coenda V., Martínez H. J., Muriel H., Lapi A., 2024, *arXiv e-prints*, p. arXiv:2410.05385  
 Pattarakijwanich P., Strauss M. A., Ho S., Ross N. P., 2016, *ApJ*, **833**, 19  
 Pawlik M. M., et al., 2018, *MNRAS*, **477**, 1708  
 Poggianti B. M., Wu H., 2000, *ApJ*, **529**, 157  
 Quintero A. D., et al., 2004, *ApJ*, **602**, 190

Rosa-González D., Terlevich E., Terlevich R., 2002, *MNRAS*, **332**, 283  
 Rosario D. J., Mendel J. T., Ellison S. L., Lutz D., Trump J. R., 2016, *MNRAS*, **457**, 2703  
 Rowlands K., Wild V., Nesvadba N., Sibthorpe B., Mortier A., Lehnert M., da Cunha E., 2015, *MNRAS*, **448**, 258  
 Salim S., et al., 2016, *ApJS*, **227**, 2  
 Smail I., Morrison G., Gray M. E., Owen F. N., Ivison R. J., Kneib J. P., Ellis R. S., 1999, *ApJ*, **525**, 609  
 Stasińska G., Cid Fernandes R., Mateus A., Sodré L., Asari N. V., 2006, *MNRAS*, **371**, 972  
 Stasińska G., et al., 2008, *MNRAS*, **391**, L29  
 Stoughton C., et al., 2002, *AJ*, **123**, 485  
 Strauss M. A., et al., 2002, *AJ*, **124**, 1810  
 Taylor M. B., 2005, in Shopbell P., Britton M., Ebert R., eds, *Astronomical Society of the Pacific Conference Series Vol. 347, Astronomical Data Analysis Software and Systems XIV*. p. 29  
 Vale Asari N., et al., 2020, *MNRAS*, **498**, 4205  
 Valiante E., et al., 2016, *MNRAS*, **462**, 3146  
 Vazdekis A., Sánchez-Blázquez P., Falcón-Barroso J., Cenarro A. J., Beasley M. A., Cardiel N., Gorgas J., Peletier R. F., 2010, *MNRAS*, **404**, 1639

Werle A., Cid Fernandes R., Vale Asari N., Bruzual G., Charlot S., Gonzalez Delgado R., Herpich F. R., 2019, *MNRAS*, **483**, 2382  
 Wild V., Kauffmann G., Heckman T., Charlot S., Lemson G., Brinchmann J., Reichard T., Pasquali A., 2007, *MNRAS*, **381**, 543  
 Wild V., Charlot S., Brinchmann J., Heckman T., Vince O., Pacifici C., Chevallard J., 2011, *MNRAS*, **417**, 1760  
 Worthey G., Ottaviani D. L., 1997, *ApJS*, **111**, 377  
 Wright E. L., et al., 2010, *AJ*, **140**, 1868  
 Wright A. H., et al., 2016, *MNRAS*, **460**, 765  
 Yan R., et al., 2009, *MNRAS*, **398**, 735  
 Yesuf H. M., French K. D., Faber S. M., Koo D. C., 2017, *MNRAS*, **469**, 3015  
 Zabludoff A. I., Zaritsky D., Lin H., Tucker D., Hashimoto Y., Shectman S. A., Oemler A., Kirshner R. P., 1996, *ApJ*, **466**, 104  
 da Cunha E., Charlot S., Elbaz D., 2008, *MNRAS*, **388**, 1595

## APPENDIX

### A. STAR FORMATION HISTORIES FOR TOY SED MODELS

To create our toy SED models we selected galaxies from the STARLIGHT-SDSS catalogue which belong to the SDSS main galaxy sample, with a signal-to-noise ratio  $S/N \geq 10$  at  $4020 \text{ \AA}$ ,  $M_* \geq 10^7 M_\odot$  and non-negative Petrosian half-light radius, which results in a parent sample of 616,097 objects. The star-forming sample comprises 133,769 galaxies below the Stasińska et al. (2006) line and with  $W_{H\alpha} \geq 3 \text{ \AA}$ . Our subsample of 314,880 retired galaxies is defined as those with  $W_{H\alpha} < 3 \text{ \AA}$ , while the 580 post-starburst were selected using the Goto (2007) criteria.

Figure A1 shows the average STARLIGHT fitted star formation histories (SFH) of our star-forming, post-starburst and retired galaxy subsamples split into five stellar mass bins. These are displayed in cumulative form, in order to best highlight the differences between the different subsamples. These average star formation histories are used to calculate  $L_{TIR}$  and  $L_{H\alpha}$  in our toy models, as described in Section 5. We excluded the two lowest mass bins for the retired and post-starburst samples, due to the low number of galaxies or very low predicted luminosities.

We can see that retired galaxies have been quiescent for at least 1 Gyr, at all stellar masses. Post-starburst galaxies experienced a significant burst of star formation between 500 and 1.5 Gyr ago and have undergone minimal star formation since. Low mass star-forming galaxies show substantial star formation within the past 1 Gyr, while higher mass galaxies formed an increasingly insignificant proportion of their mass recently. These star formation histories demonstrate that the star formation rate of all galaxies with stellar masses larger than  $10^9 M_\odot$ , as in our samples (Figure 1), has been very stable for the last 100 Myr. This is important for our discussion of the cause of the excess  $L_{TIR}$  in the retired and post-starburst galaxies in Section 5.

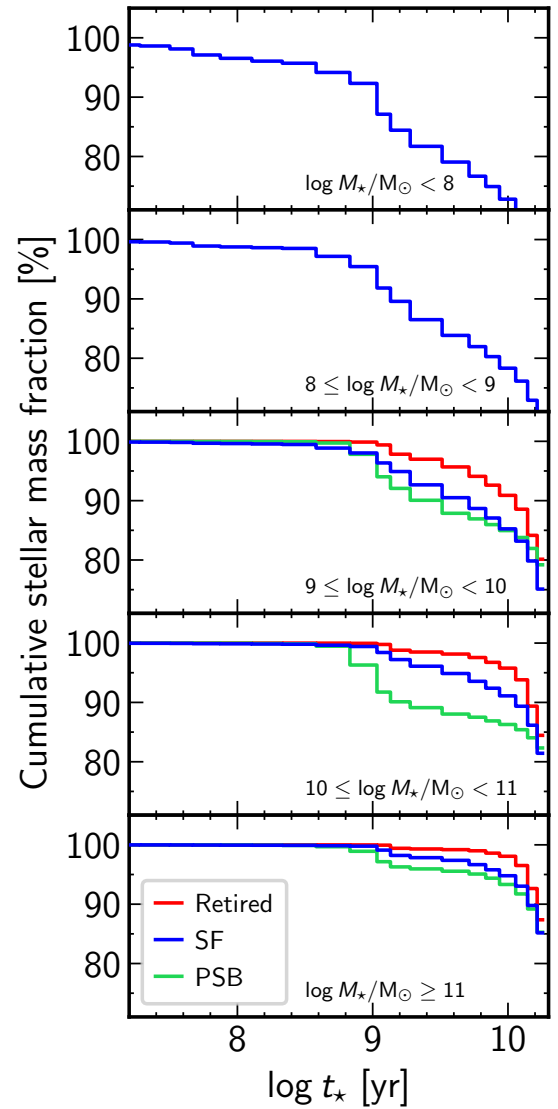


**Figure A1.** Average star formation histories for the retired, post-starburst (PSB) and star-forming (SF) subsamples in stellar mass bins, used in the toy models in Section 5. The cumulative star formation rate is shown as function of the stellar population age  $t_*$ .

Our conversion from star formation history into  $L_{\text{TIR}}/L_{\text{H}\alpha}$  depends on many properties of the stellar population models and dust attenuation curve, and the magnitude of the effect in Figure 4 should only be taken as indicative. We investigated the impact of changing the assumed attenuation curve to a shallower Charlot & Fall (2000) dust law, with  $q_{\lambda} = (\lambda/5500 \text{ \AA})^{-0.7}$ . This results in a modest increase in the predicted  $\log L_{\text{TIR}}$  of 0.16 dex for the star-forming and of 0.08 dex for the post-starburst and retired galaxies. More recent stellar population models than the BC03 models used here yield slightly different SFHs when fit to optical spectra, e.g. a newer version of the Bruzual & Charlot models which include the new MILES stellar spectral library result in smoother SFHs (e.g. Pawlik et al. 2018). Improvements in UV modelling post-Bruzual & Charlot (2003) may slightly shift our results, but the key challenge lies in accurately characterizing young stellar populations. From a technical perspective, incorporating UV constraints into optical spectral synthesis can help to better constrain these populations (e.g. López Fernández et al. 2018; Werle et al. 2019). However, even the latest stellar libraries face limitations, particularly in their coverage of the crucially important hot young stars. Excluding stellar populations younger than  $10^8$  years from our calculations is not ideal, as these do contribute some light to the galaxy SED, if not much mass. However, excluding these ages is a common approach taken to account for these limitations, with some stellar population models only starting at 30–60 Myr (e.g. Vazdekis et al. 2010).

This paper was built using the Open Journal of Astrophysics L<sup>A</sup>T<sub>E</sub>X template. The OJA is a journal which provides fast and easy peer review for new papers in the **astro-ph** section of the arXiv, making the reviewing process simpler for authors and referees alike. Learn more at <http://astro.theoj.org>.